Anomalous Cracking in a Metal-Organic Framework Glass

Malwina Stepniewska[1], Kacper Januchta[1], Chao Zhou[1], Ang Qiao[1,2], Morten M. Smedskjaer[1] and Yuanzheng Yue[1,2]

[1]Department of Chemistry and Bioscience, Aalborg University, DK-9220 Aalborg, Denmark

[2] State Key Laboratory of Silicate Materials for Architectures, Wuhan University of Technology, Wuhan 430070, China

Correspondence and requests for materials should be addressed to Y.Z.Y. (email: yy@bio.aau.dk).

Abstract

Metal-organic framework (MOF) glasses is a newly discovered family of melt-quenched glasses. Recently, several intriguing features (e.g., ultrahigh glass forming ability and low liquid fragility) have been discovered in the glasses obtained from zeolitic imidazolate frameworks (ZIFs) that are a subset of MOFs. However, the fracture behavior of ZIF glasses remains elusive. Here, we report on the first important finding, namely, the anomalous crack behavior in a representative ZIF glass, i.e., ZIF-62 glass with the chemical composition of $ZnIm_{2-x}bIm_x$, where the central node – zinc - is coordinated to imidazolate (Im) and benzimidazole (bIm) ligands. By performing micro- and nano-indentation and atomic force microscopy (AFM) analysis, we observe a unique sub-surface cracking phenomenon with induced shear bands on the indent faces, in contrast to the cracking behavior of other types of network glasses. The occurrence of shear bands could be attributed to the breakage of coordinative bonds that are much weaker than ionic and covalent The observed anomalous cracking behavior accords with the high Poisson's ratio (=0.34) of the ZIF-62 glass.

Metal-organic frameworks (MOFs) are composed of metal nodes and organic linkers. An important subset of MOFs is the zeolitic imidazolate frameworks (ZIFs), which exhibit higher thermal and chemical stability than other subsets[1,2]. Like silica or zeolites, ZIFs have a three-dimensional network

structure, which is constituted by the interconnected metal-ligand tetrahedra. The tetrahedron consists of one central transition metal and four imidazolate ligands[3–6]. Recently, it was discovered that some ZIFs can be melted and subsequently quenched to the glassy state prior to thermal decomposition[7–12]. This new family of melt-quenched glasses is structurally distinct from other traditional glass families such as metallic, organic, and inorganic ones.

Despite progress in understanding the structure and properties of ZIF glasses[12–16], their mechanical properties have been studied to a very limited extent, in particular, their cracking behavior has not been reported so far. However, it is crucial to study the fracture and deformation behavior of the ZIF glasses in order to understand the nature of ZIF glasses and to find their application fields. Therefore, in the present work, we investigate the mechanical properties of ZIF glasses by using ZIF-62 glass as a representative object of our study. We chose ZIF-62 glass because it can be made to relatively large, homogeneous bulk samples for mechanical testing, and also because it has already been studied regarding its structure[10] and several properties[11,15,16].

ZIF-62 ($Zn(Im)_{2-x}(bIm)_x$) is an excellent glass former, in which the central Zn node is connected by two types of ligands: imidazole (Im) and benzimidazole (bIm), depending on the x value[2]. ZIF-62 exhibits higher thermal and structural stability in the liquid state compared to other ZIFs, e.g., a broader temperature range (about 100 K) between melting and decomposition events (Supplementary Figure 1)[8,10]. ZIF-62 glasses were found to have ultrahigh glass forming ability (T_g/T_m=0.84, where T_g is glass transition temperature and T_m is melting point) and high viscosity (~10^5 Pa s) at T_m[10], as well as structural stability upon heating[11]. The structural difference between ZIF-62 crystal and glass has recently been revealed by X-ray total scattering, Raman, and X-ray Photoelectron Spectroscopy analyses[10]. In terms of pair distribution functions, ZIF-62 crystal features high degree of intermediate (<20 Å) and long range (>20 Å) order, whereas ZIF-62 glass is

characterized by high degree of intermediate and long range disorder[10]. However, the degree of disorder of the short-range (~7 Å) structure (i.e., tetrahedral units) of ZIF glasses remains elusive[14].

In previous work, the indentation modulus of ZIF-62 glass was determined to be about 6 GPa by means of nanoindentation[8], while its Poisson's ratio was found by Brillouin scattering to be 0.44, i.e., extremely incompressible and higher than most glasses[10]. Recently, a first study of creep and scratch testing on ZIF-62 glass has been performed,[15] reporting that that its strain rate sensitivity is similar to that of glassy polymers and some chalcogenide glasses. In the present study, we perform micro- and nanoindentation on ZIF-62 glass to study its deformation and crack initiation behavior during sharp contact loading. We compare the hardness values of ZIF-62 glass with those of metallic and oxide glasses. We attempt to clarify both the sub-surface cracking mechanism of ZIF-62 glass under sharp contact loading, and its deformation behavior during nanoindentation.

Results

Figure 1a shows the obtained Vickers indent impressions, suggesting the occurrence of sink-in in the ZIF glass, i.e., deformation downward with respect to the sample surface. A change in the crack pattern with increasing load can be observed, i.e., the crack density increases with increasing load, with radial cracks initiating at the highest loads (0.5 N). The crack resistance, as determined from the load at 50% probability of initiation of radial cracks[17], is estimated to be around 2 N (Figure 1b, red points). The micro-indentation data are also used to calculate Vickers hardness. As shown in Figure 1b, the hardness first decreases drastically from 0.65 to 0.53 GPa with increasing load from 0.1 to 0.2 N, and then gradually decreases from 0.53 to 0.50 GPa for higher indentation loads. The first stage of the hardness drop could be ascribed to the collapse of the surface defects (e.g., voids) by slightly increasing load, leading to large volume deformation without significant bond breakage[18]. The second stage is expected to be due to the indentation size effect[19,20], which has been attributed to

an increased ratio between indentation surface and deformation volume with decreasing load, i.e., to the fact that the elastic contribution to the total deformation caused by indentation becomes larger at lower load[21,22].

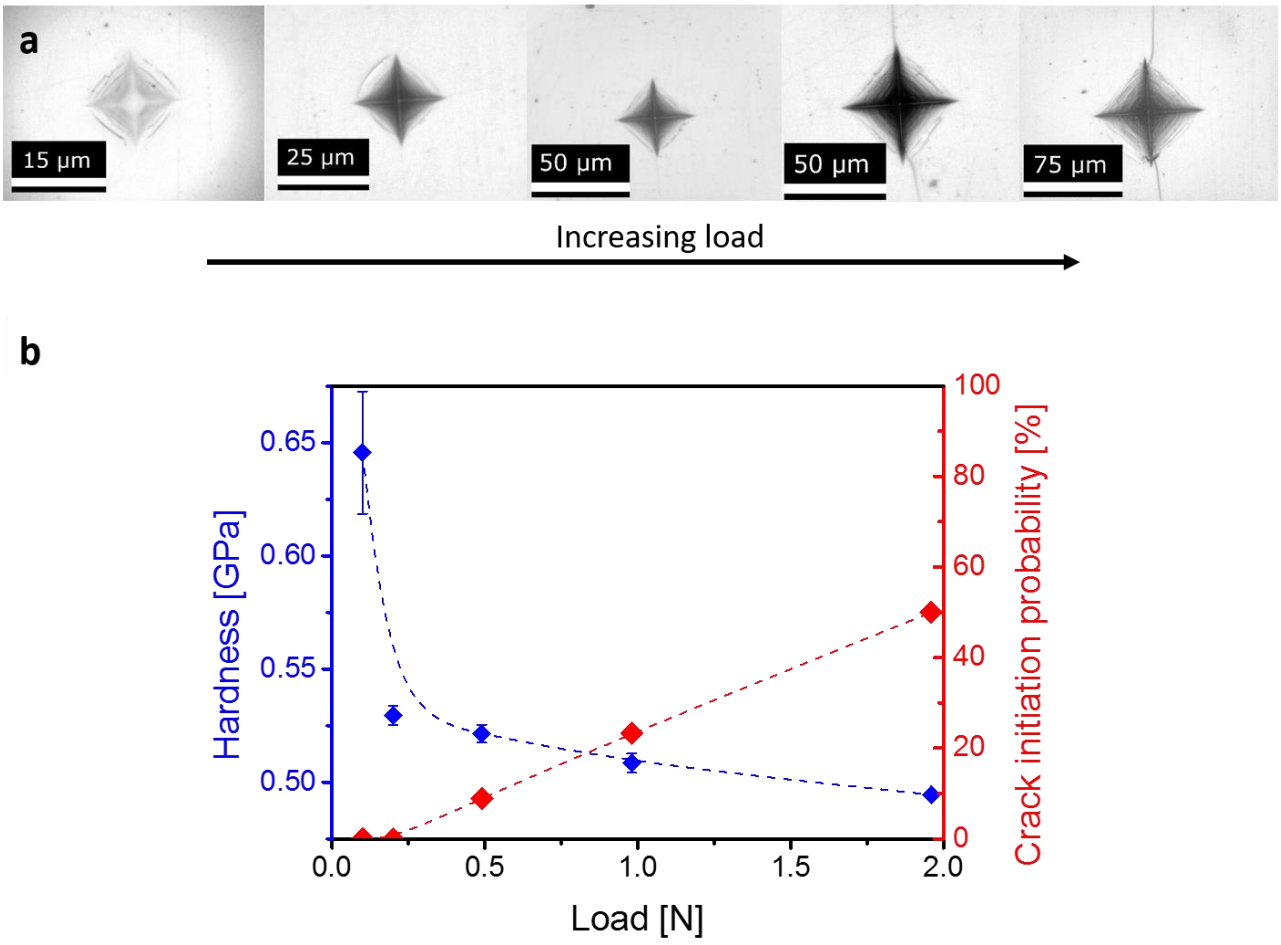

Figure 1. Indentation behavior and Vickers microhardness for ZIF-62 glass in the load range of 0.1 to 1.96 N. (a) Indent images (note the different scale) for increasing load as shown by the arrow. (b) Microhardness (blue points) and crack initiation probability (red points) as a function of applied load. The dashed lines are guides for the eyes.

Figure 2a shows the optical images of the cross-section of an indent along one horizontal crack (see inset) generated under the maximum load of 5 N for the ZIF-62 glass. The sub-surface area can be divided into three main zones, as marked in Figure 2a, in order to study the crack initiation and material deformation mechanisms[23]. Zone I refers to the process zone (i.e., densified region or plastic contact zone), which is located below the visible indent and constitutes a strongly deformed plastic contact zone with a clear hemispherical boundary (denoted as A). In Zone I, we also observe micro-cracks originating at the surface (see green ellipse). The micro-cracks will be further illustrated in Figure 3. Zone II is the nearly spherical elastic zone[24,25], which lies between Zone I and the un-deformed glass matrix. In this zone, both median and radial cracks can be observed. The median crack initiates at point B and then propagates further as indicated by C (see the red circles in Figure 2a). The radial cracks occur as a semi-circle (indicated by D). Zone III is the semi-spherical domain, which is situated outside Zone II and is bordered by the glass matrix that is not subjected to deformation during indentation. The occurrence of the three zones is a typical feature of most silicate glasses [23,26], which are topologically similar, despite the difference in bond strength, to the present ZIF-62 glass due to the tetrahedral O-Si-O and Im-Zn-bIm building units in the former and latter, respectively. As shown in Figure 2b, the standard soda lime silica (SLS) window glass, included for comparison, exhibits a similar fracture patterns as the ZIF-62 glass.

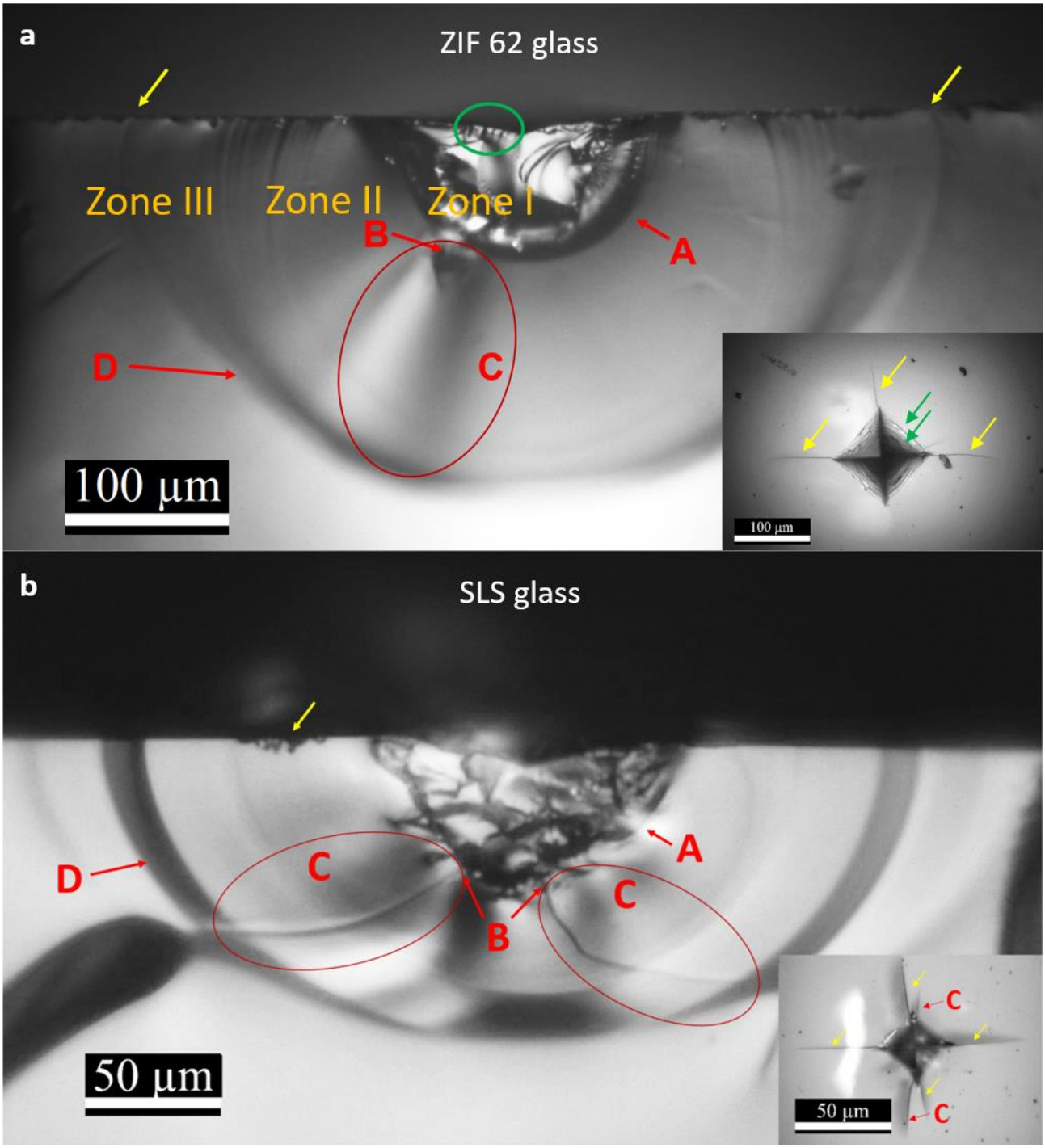

Figure 2. Cross-section view of an indentation deformed zone on (a) ZIF-62 glass and (b) soda-lime-silica (SLS) glass after loading with maximum force of 5 N, showing different sub-surface features: A – strongly deformed plastic zone; B – initiation point of the median crack; C – propagation zone of the median crack; D – radial crack; yellow arrows – points at which radial cracks reach surface of

the sample; green elipse – examples of the lines visible inside indents, corresponding to shear bands and edge cracks. Inset: top view of an indent with radial cracks (yellow arrows) and lines visible inside the indent (examples shown with green arrows) and median cracks for SLS glass (red arrows, C).

Figure 3a shows the optical top view image of an indent formed in the ZIF-62 glass under the load of 1.96 N, where we observe a layered indent pattern. In the domain marked by the red square frame, we recorded an AFM image, showing two distinct cracking features: shear band formation (designated as A) and edge cracking (designated as B) as shown in Figure 3b. Shear bands or slip lines, which are narrow regions of excessive strain, are typically observed in metallic glasses[27–29], but have also been reported in some modified oxide glasses[24]. Remarkably, we are here able to identify the scale of the shear band, i.e., a shear-induced dislocation of 35 nm as indicated in Figure 3c. In other words, we discovered a step-like structural sliding at the nano-scale within the deformation zone in the ZIF-62 glass upon indentation. To the best of our knowledge, this has never been observed before in network glasses with fully polymerized structure, completely corner-shared or bridged tetrahedral network, such as that of pure silica glass. The origin of the step-like crack will be discussed in the next section. Small chipped domains on the sample surface are clearly visible as the end of the radial cracks (yellow arrows on Figure 2). In Figure 3a, we also notice that the radial cracks do not originate from the corners of indents, but from the first-formed edge cracks.

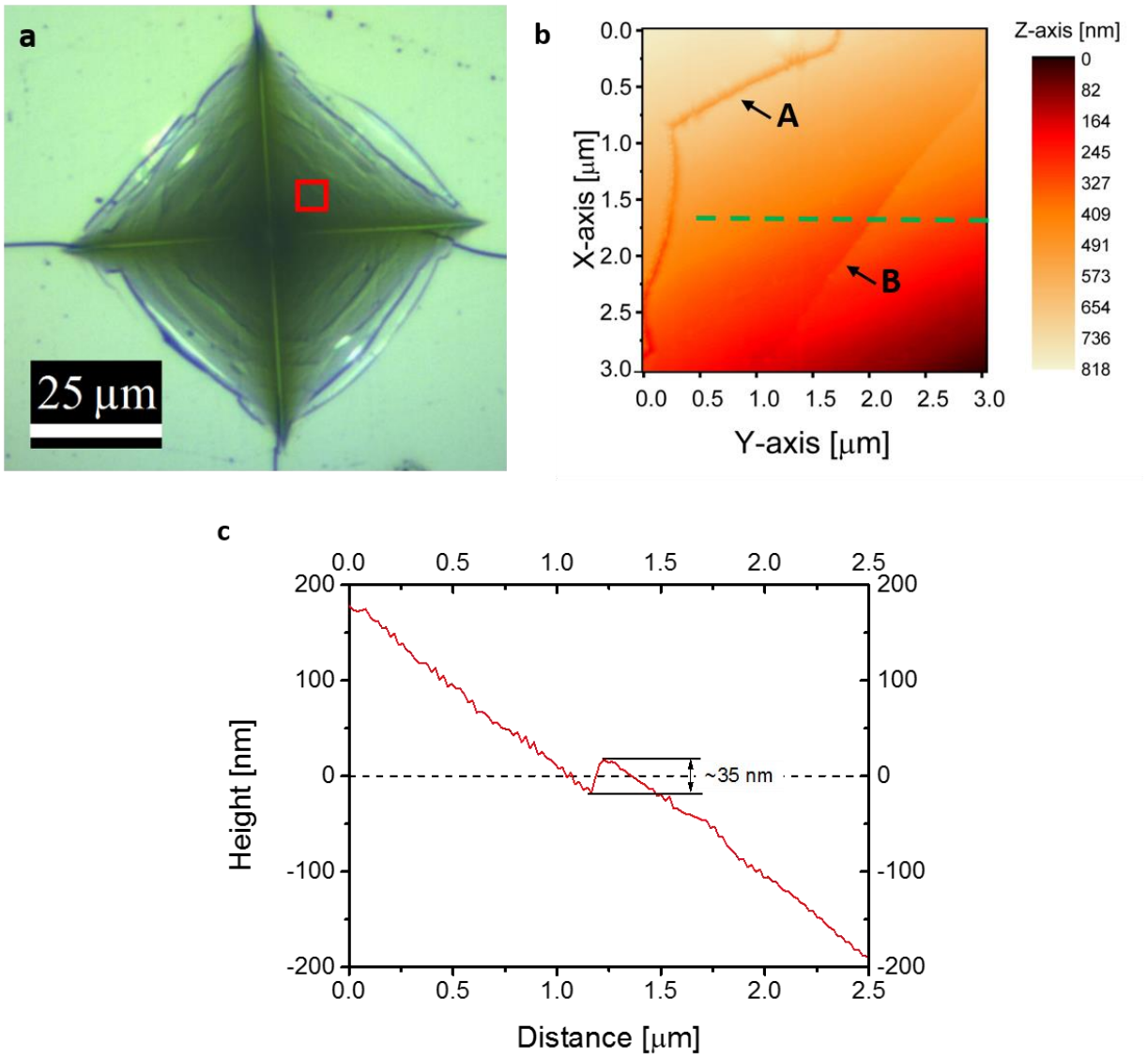

Figure 3. Atomic force microscopy (AFM) measurements on the indent walls (at 1.96 N) of the ZIF-62 glass. (a) Optical microscopy image of 1.96 N indent, with the red square showing the AFM scanned area. (b) Two-dimensional height profile of the AFM scanned area, showing a crack (designated as A) and a shear band (designated as B). Note the change of height in the vicinity of the observed shear band. The dashed green line shows the line scan used to make the height profile in subfigure c. (c) AFM height profile of line scan passing through a shear band, showing an increase in height of around 35 µm at the location of the shear band.

Figure 4 shows the nanoindentation data, from which we find a decreasing trend in both hardness and indentation modulus with increasing load, similar to that for Vickers microhardness (Figure 1b). The E_{ind}/H_{nano} ratio is about 8.2 at the load of 0.01 N, and then slightly increases to a constant value of 8.5 with increasing load (Figure 4a). Similarly to the microindentation impressions (Figure 1a), the nanoindentation impressions after unloading exhibit linearly aligned patterns parallel to the indent edges, being either edge cracks or shear bands (Supplementary Figure 2). The load–displacement curves (Supplementary Figure 3) have been analyzed to determine the relative elastic and plastic work (see method in Supplementary Figure 4), as well as the relative elastic and plastic displacement during indentation (Supplementary Table 1). An elastic deformation of about 50% is estimated for all the applied loads, implying rather high contribution of elastic deformation to the total deformation induced by indentation loading, e.g., compared to most oxide glasses[30]. Based on the AFM indent shape analysis (Figure 4b), only a slight pile-up contribution can be observed in the vicinity of the indents. Observation of pile-up around the indent edges would have been indicative of activated isochoric shear flow during indentation[31]. As such, this is an interesting observation when considering the pronounced presence of shear bands inside the indents, suggesting that plastic deformation, i.e., translational motion of structural units driven by breakage of the Zn-N bonds, is highly localized in the ZIF glass.

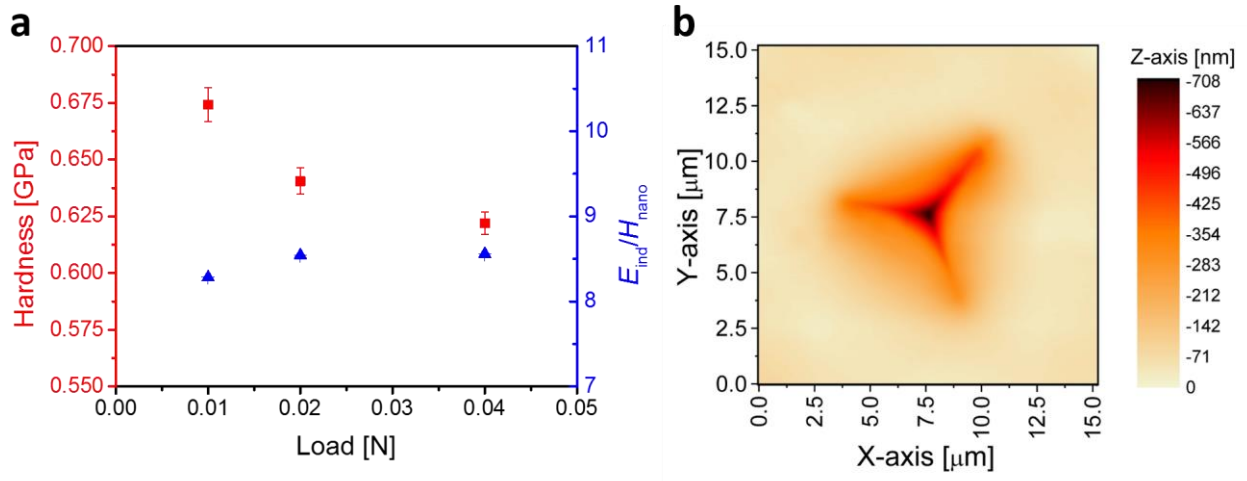

Figure 4. Mechanical properties of ZIF-62 glass as determined by nanoindentation and the nano-indent image obtained by AFM. (a) Hardness (red points) and indentation modulus normalized by nanohardness (E_{ind}/H_{nano}, blue points) as a function of applied load. (b) Topographical AFM image of the indent produced under the load of 0.01 N. Note the slight pile-up in the vicinity of the indent.

Finally, based on measurements of the longitudinal and transverse sound wave velocities, we calculated the Poisson's ratio of the ZIF-62 glass to be 0.345. This value is significantly lower than that recently measured by Brillouin scattering (0.44)[10].

Discussion

From Figure 1, the hardness of bulk ZIF-62 glass lies in the range of 0.5-0.65 GPa, thus much softer than inorganic network glasses, e.g., oxide glasses that possess a range of hardness of 3-9 GPa[32]. The much lower hardness of ZIF glasses could be attributed to the four following aspects.

First, the three-dimensional ZIF network is constructed through the coordinative bonds between the metal nodes and the N atoms of imidazolate and benzimidazolate ligands. Such bonds are much weaker than, e.g., the Si-O bonds in inorganic network glasses. For instance, to break the coordinative

bonds of ZIF-4, that is a glass with similar bond structure to ZIF-62, an energy barrier of 81 kJ/mol needs to be overcome[33]. In contrast, 443 kJ/mol is required to break the Si-O bonds[34]. Consequently, the resistance of the ZIF glasses to plastic deformation is significantly lower than that of the oxide glasses.

Second, the density of the topological bond constraints, i.e., the number of bond stretching and bond bending constraints per unit of volume in ZIF glasses is much lower than that in oxide glasses. This is because the volume of the tetrahedral unit $Zn(Im)_4$ of ZIF-62 is considerably larger (about 6 Å distance for Zn-N-N-Zn[8,10,11,14]) than that of oxide glasses (e.g., 3 Å distance for Si-O-Si[35,36]) for the same number of linear and angular constraints. It is known that the glass hardness decreases with decreasing volumetric constraint density[37]. Thus, the ZIF glasses are softer than the oxide glasses. The detailed calculation of the constraint density will be conducted in a separate work.

Third, ZIF glasses possess a large fraction of organic ligand molecules, which have a higher degree of rotational and translational freedom, e.g., compared to the rigid oxide network consisting of $[SiO_4]$ units. Therefore, ZIF glasses are more deformable than oxide glasses upon indentation.

Fourth, ZIF materials feature a large amount of free volume, i.e., voids. Despite the collapse and disordering of those voids in the glassy state, the free volume is still much larger than that of oxide glasses. The larger fraction of voids leads to lowering of the deformation resistance[38–42].

Considering next the cracking pattern of the ZIF glass, we note that median and radial cracking is observed, similarly to most oxide glasses such as SLS glass (Figure 3). This correlates well with relatively high Poisson's ratio of ZIF glasses[43], yet not with the low elastoplastic E/H ratio which usually promotes ring cracking instead of radial cracking[31,40,43]. The lack of pronounced indent edges in the ZIF-62 glass suggests that sinking-in occurs during loading, while the observed indent shape itself implies a high contribution of elastic deformation to the indentation deformation[44,45]. As further

observed from the indent cross-section (Figure 2) and AFM measurements on the indent walls (Figure 3), we have discovered an interesting, anomalous micro-cracking behavior for the ZIF-62 glass, i.e., shear band formation with discrete jump on the height profile of the indent wall caused by indentation. By 'anomalous', we mean that this phenomenon has not been found in any other fully polymerized 3D network glasses. The non-network metallic glasses and some depolymerized oxide glasses feature shear bands[24,27–29], but, to our best knowledge, not with the step-like height. The latter type of shear bands have, however, been observed in some chalcogenide glasses[46]. Those typical glasses possess chain-like network structure, with van der Waal's bonding between the chains, effectively lowering the resistance to deformation upon indentation[46]. However, the microscopic origin of the shear band formation in the present ZIF glass is distinct from that in the chalcogenide glasses.

The shear band formation at the nanoscale is herein verified by the sudden shift of the deformation curve, as measured by AFM (Figure 3c). The shear bands imply that the step-like micro-crack is accompanied by a step-like structural sliding upon indentation. Its origin should be associated with the weak coordinative bonds that can easily be broken by applying a small shear stress compared to the ionic-covalent Si-O bonds. The covalent bonds of the ligand molecules in ZIFs are not easily broken during melting, i.e., they remain intact as evidenced by solid state ^{13}C-^{1}H coupling NMR results[8,10].

In summary, we have investigated the indentation behavior of ZIF-62 glass by performing micro- and nanohardness measurements. This typical ZIF glass is characterized by relatively low hardness, indentation modulus, and elastoplastic ratio, compared to other types of 3D network glasses, e.g., oxide glasses. We have attributed the lower hardness of ZIF glasses to four distinct structural features. We have also discovered the shear band formation during indentation and ascribed it to the weak coordinative bonds and consistent with the relatively high Poisson's ratio of ZIF glasses.

Moreover, the ZIF glass exhibits a high degree of elastic deformation, and only a slight amount of pile-up is detected, implying a high degree of densification during indentation.

Acknowledgements

This work was supported by VILLUM FONDEN under research grant no. 13253. The authors are grateful to Grethe Winther (Technical University of Denmark) for her help with nanoindentation and Haizheng Tao (Wuhan University of Technology) for facilitating sample production and valuable discussions.

Method

Sample preparation. ZIF-62 was synthesized by using the solvothermal method with the Zn:Im:bIm molar ratio of 1:8.5:1.5, which gave the final composition of ZIF-62 crystal $Zn(Im)_{1.68}(bIm)_{0.32}$ based on the relation between the designed and measured Im/bIm ratio reported elsewhere[10]. To achieve this ratio, we mixed 17.453 ml of 0.6 molar zinc nitrate hexahydrate ($Zn(NO_3)_2 \cdot 6H_2O$) (Merck), 33.816 ml of 4 molar imidazole ($C_3H_4N_2$) (Merck), and 21.817 ml of 0.5 molar benzimidazole ($C_7H_6N_2$) (Merck) solutions in N,N-dimethylformamide (DMF) (VWR). This mixture was then magnetically stirred for 1 hour. Afterwards, the solution was moved to a sealed glass jar (100 ml) and placed in a furnace for 48 hours at 403 K. The derived crystals were washed three times in DMF and finally once in dichloromethane (DCM) (Merck). The obtained product was dried at room temperature in a fume hood.

In order to prepare bulk ZIF-62 glass samples for the mechanical testing, we applied a novel processing method, i.e., hot-press method[16]. The as-prepared crystalline ZIF-62 powder was first put into a metal mould with 10 mm inner diameter. Subsequently, the mould was placed into the hot-press machine (Hefei Kejing Materials Technology Co., Ltd., China), in which the sample was

compressed under the pressure of 50 MPa and afterwards heated under vacuum to 833 K at 5 K/min and held for 30 min. Then, the liquid was cooled down to room temperature, resulting in vitrification. During the hot-press process, the applied pressure and vacuum help, respectively, to remove the bubbles from ZIF-62 melt and prevent the sample from oxidation at high temperature. Finally, we obtained a 10 mm bulk transparent homogeneous ZIF-62 glass sample without visible bubbles. Samples for indentation measurements were embedded in resin (Struers epofix), grinded using SiC paper of grit size 600, 800, 1200, 2400, and 4000, and finally polished using a suspension of diamond particles with decreasing size (3, 1, and 0.25 μm).

Mechanical characterization. Vickers microindentation was performed using Nanovea CB500 Hardness Tester with loads of 0.1, 0.2, 0.49, 0.98, and 1.96 N to observe the change of microhardness with load and to study the cracking mechanism. The Vickers diamond indenter is a square pyramid with opposite faces at an angle of 136°. For each load, a duration of 6 seconds was needed to obtain maximum load, while the time of unloading was 60 seconds. The maximum load was kept for 15 seconds. In addition to calculating Vickers hardness, we also calculated the probability of crack initiation under loads based on the obtained indent images, which was defined as the ratio between the number of observed cracks and that of indent corners (i.e., four corners per indent). The load corresponding to the crack initiation probability of 50% was considered to be the crack resistance (CR)[47].

We examined the crack pattern and shape of the sub-surface indent on both ZIF-62 glass and soda-lime-silica (SLS) window glass. The composition of SLS is $13Na_2O – 6MgO – 10CaO – 71SiO_2$ in mol% and was obtained from Velux. We compare the crack pattern of ZIF-62 glass to SLS glass, since that of the latter is well-known and characteristic of so-called “normal” oxide glasses, exhibiting long radial cracks from the indent corners[48]. To view the indent cross-sections of both glass samples, we generated a line of indents with a distance of 1.5 times the indent size between indents using the

maximum load of 5 N. The samples were then broken to get fresh fracture surfaces passing through the indents. The cross-sections were observed using an optical microscope with the total magnification of 200x.

To access the deformation patterns, hardness and apparent elastic modulus of ZIF-62 glass were measured under smaller load (<0.1 N). This was done using nanoindentation (CSM nanoindentation tester) with Berkovich tip under maximum loads of 10, 20, and 40 mN. The Berkovich diamond indenter is a three-sided pyramid with the same ratio of project area to depth as the Vickers indenter. The indenter was calibrated using a standard sample of fused silica. The obtained indentation data were analyzed based on the Oliver-Pharr method[49].

Atomic force microscopy (AFM) measurements were performed using an Ntegra (NT MDT) instrument and silicon tip cantilevers (NSG10, NT-MDT) in semi-contact mode in order to explore the deformation mechanisms of ZIF-62 glass under contact loading. Due to the large size of the Vickers microindents, only selected areas (~3×3 μm^2) were imaged, while 10 mN nanoindents were imaged in their entirety (~15×15μm^2). The scanning frequency was adjusted according to the size of the topographical image, with the scanning velocity of 3 μm/s for ~15×15μm^2 areas and 1 μm/s for the smaller areas. All AFM images have a resolution of 256×256 pixels.

Non-destructive ultrasonic method was used to measure Poisson's ratio based on the transverse and longitudinal wave propagation velocities using 38DL Plus (Olympus) ultrasonic thickness gage. This enabled obtaining the transverse (V_t) and longitudinal (V_l) wave velocities, based on the thickness of the sample (measured using digital micrometer) Based on the ultrasonic measurements performed with 20 MHz delay line transducers, Poisson's ratio (ν) was then calculated based on equation 1.

$$\nu = \frac{{V_l}^2 - 2{V_t}^2}{2({V_l}^2 - {V_t}^2)} \qquad (1)$$

References

1. Park, K. S. *et al.* Exceptional chemical and thermal stability of zeolitic imidazolate frameworks. *Proc. Natl. Acad. Sci. U. S. A.* **103,** 10186–10191 (2006).

2. Gustafsson, M. & Zou, X. Crystal formation and size control of zeolitic imidazolate frameworks with mixed imidazolate linkers. *J. Porous Mater.* **20,** 55–63 (2013).

3. Liu, Y., Kravtsov, C., Larsen, R. & Eddaoudi, M. Molecular building blocks approach to the assembly of zeolite-like metal – organic frameworks (ZMOFs) with extra-large cavities. *Chem. Commun.* 1488–1490 (2006). doi:10.1039/b600188m

4. Huang, X., Lin, Y., Zhang, J. & Cheng, X.-M. Ligand-Directed Strategy for Zeolite-Type Metal– Organic Frameworks: Zinc(II) Imidazolates with Unusual Zeolitic Topologies. *Angew. Chemie* **45,** 1557–1559 (2006).

5. Zhang, J. & Chen, X. Crystal engineering of binary metal imidazolate and triazolate frameworks. *Chem. Commun.* **16,** 1689–1699 (2006).

6. Tan, J., Bennett, T. D. & Cheetham, A. K. Chemical structure, network topology, and porosity effects on the mechanical properties of Zeolitic Imidazolate Frameworks. *Proc. Natl. Acad. Sci. U. S. A.* **107,** 9938–9943 (2010).

7. Bennett, T. D. *et al.* Hybrid glasses from strong and fragile metal-organic framework liquids. *Nat. Commun.* **6,** 8079 (2015).

8. Bennett, T. D. *et al.* Melt-Quenched Glasses of Metal-Organic Frameworks. *J. Am. Chem. Soc.* **138,** 3484–3492 (2016).

9. Tao, H., Bennett, T. D. & Yue, Y. Melt-Quenched Hybrid Glasses from Metal–Organic Frameworks. *Adv. Mater.* **29,** 1601705 (2017).

10. Qiao, A. *et al.* A metal-organic framework with ultrahigh glass-forming ability. *Sci. Adv.* **4,** eaao6827 (2018).

11. Zhou, C. *et al.* Thermodynamic features and enthalpy relaxation in a metal–organic framework glass. *Phys. Chem. Chem. Phys.* **20,** 18291–18296 (2018).

12. Longley, L. *et al.* Liquid phase blending of metal-organic frameworks. *Nat. Commun.* **9,** 2135 (2018).

13. Zhou, C. *et al.* Metal-organic framework glasses with permanent accessible porosity. *Nat. Commun.* **9,** 5042 (2018).

14. Zhang, J. *et al.* Structural Evolution in a Melt-Quenched Zeolitic Imidazolate Framework Glass during Heat-treatment. *Chem. Commun.* **55,** 2521–2524 (2019).

15. Li, S. *et al.* Mechanical Properties and Processing Techniques of Bulk Metal-Organic Framework Glasses. *J. Am. Chem. Soc.* **141,** 1027–1034 (2018).

16. Qiao, A. *et al.* Optical properties of a melt-quenched metal-organic framework glass. *Opt. Lett.* **44,** (2019).

17. Wada, M., Furukawa, H. & Fujita, K. Crack resistance of glass on Vickers indentation. *Proc. X Int. Congr. Glas.* **11,** 39–46 (1974).

18. Manika, I. & Maniks, J. Size effects in micro- and nanoscale indentation. *Acta Mater.* **54,** 2049–2056 (2006).

19. Farges, G. & Degout, D. Interpretation of the indentation size effect in vickers microhardness measurements-absolute hardness of materials. *Thin Solid Films* **181,** 365–374 (1989).

20. Gong, J., Wu, J. & Guan, Z. Examination of the Indentation Size Effect in Low-load Vickers Hardness Testing of Ceramics. *J. Eur. Ceram. Soc.* **19,** 2625–2631 (1999).

21. Li, H. & Bradt, R. C. The microhardness indentation load/size effect in rutile and cassiterite single crystals. *J. Mater. Sci.* **28,** 917–926 (1993).

22. Kavetskyy, T., Borcc, J., Sangwal, K. & Tsmots, V. Indentation size effect and Vickers microhardness measurement of metal-modified arsenic chalcogenide glasses. *J. Optoelectron. Adv. Mater.* **12,** 2082–2091 (2010).

23. Atkinson, C., Martínez-Esnaola, J. M. & Elizalde, M. R. Contact mechanics: a review and some applications. *Mater. Sci. Technol.* **28,** 1079–1091 (2012).

24. Gross, T. M., Wu, J., Baker, D. E., Price, J. J. & Yongsunthon, R. Crack-resistant glass with high shear band density. *J. Non. Cryst. Solids* **494,** 13–20 (2018).

25. Gross, T. M. & Tomozawa, M. Indentation-induced microhardness changes in glasses: Possible fictive temperature increase caused by plastic deformation. *J. Non. Cryst. Solids* **354,** 4056–4062 (2008).

26. Sglavo, V. M. & Green, D. J. Subcritical Growth of Indentation Median Cracks in Soda-Lime-Silica Glass. *J. Am. Ceram. Soc.* **78,** 650–656 (1995).

27. Greer, A. L., Cheng, Y. Q. & Ma, E. Shear bands in metallic glasses. *Mater. Sci. Eng. R Reports* **74,** 71–132 (2013).

28. Egami, T., Iwashita, T. & Dmowski, W. Mechanical Properties of Metallic Glasses. *Metals (Basel).* **3,** 77–113 (2013).

29. Lu, Y. M. *et al.* Shear-banding Induced Indentation Size Effect in Metallic Glasses. *Sci. Rep.* **6,** 1–12 (2016).

30. Yamane, M. & Mackenzie, J. D. Vicker's Hardness of glass. *J. Non. Cryst. Solids* **15,** 153–164 (1974).

31. Januchta, K. & Smedskjaer, M. M. Indentation deformation in oxide glasses: Quantification, structural changes, and relation to cracking. *J. Non-Crystalline Solids X* **1,** 100007 (2019).

32. Januchta, K. *et al.* Discovery of Ultra-Crack-Resistant Oxide Glasses with Adaptive Networks. *Chem. Mater.* **29,** 5865–5876 (2017).

33. Gaillac, R., Pullumbi, P. & Courdet, F.-X. Melting of Zeolitic Imidazolate Frameworks with Different Topologies: Insight from First-Principles Molecular Dynamics. *J. Phys. Chem. C* **112,** 6730−6736 (2018).

34. Clupper, D. C. & Hench, L. L. Crystallization kinetics of tape cast bioactive glass 45S5. *J. Non. Cryst. Solids* **318,** 43–48 (2003).

35. Johnson, P. A. V., Wright, A. C. & Sinclair, R. N. Neutron scattering from vitreous silica II.

Twin-axis diffraction experiments. *J. Non. Cryst. Solids* **58,** 109–130 (1983).

36. Greaves, G. N. & Sen, S. Inorganic glasses, glass-forming liquids and amorphizing solids. *Adv. Phys.* **56,** 1–166 (2007).

37. Zheng, Q., Yue, Y. & Mauro, J. C. Density of topological constraints as a metric for predicting glass hardness. *Appl. Phys. Lett.* **111,** 011907 (2017).

38. Rouxel, T. Elastic properties of glasses: a multiscale approach. *Comptes Rendus - Mécanique* **334,** 743–753 (2006).

39. Wondraczek, L. *et al.* Towards Ultrastrong Glasses. *Adv. Mater.* **23,** 4578–4586 (2011).

40. Sellappan, P. *et al.* Composition dependence of indentation deformation and indentation cracking in glass. *Acta Mater.* **61,** 5949–5965 (2013).

41. Park, K. W., Jang, J. il, Wakeda, M., Shibutani, Y. & Lee, J. C. Atomic packing density and its influence on the properties of Cu-Zr amorphous alloys. *Scr. Mater.* **57,** 805–808 (2007).

42. Cheng, Y. Q. & Ma, E. Atomic-level structure and structure-property relationship in metallic glasses. *Prog. Mater. Sci.* **56,** 379–473 (2011).

43. Rouxel, T. Driving force for indentation cracking in glass: composition, pressure and temperature dependence. *Philos. Trans. R. Soc. A Math. Phys. Eng. Sci.* **373,** 20140140 (2015).

44. Elmustafa, A. A. Pile-up/sink-in of rate-sensitive nanoindentation creeping solids. *Model. Simul. Mater. Sci. Eng.* **15,** 823 (2007).

45. Hardiman, M., Vaughan, T. J. & McCarthy, C. T. The effects of pile-up, viscoelasticity and hydrostatic stress on polymer matrix nanoindentation. *Polym. Test.* **52,** 157–166 (2016).

46. Guin, J., Rouxel, T., Sanglebœuf, J., Melscooet, I. & Lucas, J. Hardness, Toughness, and Scratchability of Germanium–Selenium Chalcogenide Glasses. *J. Am. Ceram. Soc.* **85,** 1545–1552 (2002).

47. Wada, M., Furukawa, H. & Fajita, K. Crack resistance of glass on Vickers indentation. in *Proc. Int. Congr. Glass 10th* 39–46 (1974).

48. Arora, A., Marshall, D. B., Lawn, B. R. & Swain, M. V. Indentation deformation/fracture of normal and anomalous glasses. *J. Non. Cryst. Solids* **31,** 415–428 (1979).

49. Oliver, W. C. & Pharr, G. M. An improved technique for determining hardness and elastic modulus using load and displacement sensing indentation experiments. *J. Mater. Res.* **7,** 1564–1583 (1992).